Inverted velocity profile in the cylindrical Couette flow of a rarefied gas

AUTHOR(S):

Aoki, K; Yoshida, H; Nakanishi, T; Garcia, AL

CITATION:

Aoki, K ...[et al]. Inverted velocity profile in the cylindrical Couette flow of a rarefied gas. Physical Review E 2003, 68(1): 016302.

ISSUE DATE:

2003-07

URL:

http://hdl.handle.net/2433/39905

PHYSICAL REVIEW E **68**, 016302 (2003)

Inverted velocity profile in the cylindrical Couette flow of a rarefied gas

Kazuo Aoki,* Hiroaki Yoshida, and Toshiyuki Nakanishi
Department of Aeronautics and Astronautics, Graduate School of Engineering, Kyoto University, Kyoto 606-8501, Japan

Alejandro L. Garcia
Department of Physics, San José State University, San José, California 95192-0106, USA

(Received 7 February 2003; published 11 July 2003)

The cylindrical Couette flow of a rarefied gas is investigated, under the diffuse-specular reflection condition of Maxwell's type on the cylinders, in the case where the inner cylinder is rotating whereas the outer cylinder is at rest. The inverted velocity profile for small accommodation coefficients, pointed out by Tibbs, Baras, and Garcia [Phys. Rev. E **56**, 2282 (1997)] on the basis of a Monte Carlo simulation, is investigated extensively by means of a systematic asymptotic analysis for small Knudsen numbers as well as the direct numerical analysis of the Boltzmann equation, and the parameter range in which the phenomenon appears is clarified.

DOI: 10.1103/PhysRevE.68.016302 PACS number(s): 47.45.Gx, 47.45.Nd, 51.10.+y

I. INTRODUCTION

Cylindrical Couette flow, which is a textbook example in classical fluid dynamics, is also one of the most fundamental problems in the kinetic theory of gases [1] and has been investigated from various points of view. The recent interest extends to topics such as the validity of the principle of the frame indifference [2] and the bifurcation of flows when evaporation and condensation take place on the cylinders [3–5].

One of such examples is given in a paper by Tibbs, Baras, and Garcia [6], where the cylindrical Couette flow of a rarefied gas is analyzed numerically by means of the direct simulation Monte Carlo (DSMC) method under the diffuse-specular reflection condition of Maxwell's type on the cylinders in the case where the inner cylinder is rotating whereas the outer one is at rest. Their result shows that when the accommodation coefficients of the cylinders are small (i.e., when the major part of the molecules undergo specular reflection), the flow speed of the gas increases with the distance from the inner cylinder, which is contrary to the ordinary velocity profile of the Couette flow when only the inner cylinder is rotating.

The aim of the present paper is to investigate the phenomenon of the inverted velocity profile more comprehensively and to clarify the parameter range where it appears.

II. FORMULATION OF THE PROBLEM

A. Problem

Let us consider a rarefied gas between two coaxial circular cylinders with common temperature T_0: the inner cylinder with radius r_I is rotating at a constant surface speed V_I, whereas the outer cylinder with radius r_O is at rest. Assuming the diffuse-specular reflection condition of Maxwell's type on the cylinders and restricting ourselves to the axially as well as circumferentially uniform case, we investigate the steady behavior of the gas on the basis of the Boltzmann equation. For actual numerical computation, we will assume hard-sphere molecules or the Bhatnagar-Gross-Krook (BGK) model [7,8].

B. Basic equation

We first introduce some notations: (r,θ,z) is the cylindrical coordinate system with the z axis being the axes of the cylinders; $\boldsymbol{\xi}$ is the molecular velocity and ξ_r, ξ_θ, and ξ_z are its r, θ, and z components; $f(r,\boldsymbol{\xi})$ is the velocity distribution function of the gas molecules; ρ is the density, v_r, v_θ, and v_z ($v_r=v_z=0$) are the r, θ, and z components of the flow velocity, T is the temperature, and p is the pressure of the gas; and R is the gas constant per unit mass. The dimensionless quantities corresponding to V_I, r, $\boldsymbol{\xi}=(\xi_r,\xi_\theta,\xi_z)$, f, ρ, v_θ, T, and p, which are denoted by $\hat{V}_I$, $\hat{r}$, $\boldsymbol{\zeta}=(\zeta_r,\zeta_\theta,\zeta_z)$, $\hat{f}$, $\hat{\rho}$, $\hat{v}_\theta$, $\hat{T}$, and $\hat{p}$, respectively, are defined by

$$\hat{V}_I=\frac{V_I}{(2RT_0)^{1/2}},\quad \hat{r}=\frac{r}{r_I},\quad \boldsymbol{\zeta}=\frac{\boldsymbol{\xi}}{(2RT_0)^{1/2}},$$

$$\hat{f}=\frac{(2RT_0)^{3/2}}{\rho_{av}}f,\quad \hat{\rho}=\frac{\rho}{\rho_{av}},\quad \hat{v}_\theta=\frac{v_\theta}{(2RT_0)^{1/2}},\qquad (1)$$

$$\hat{T}=\frac{T}{T_0},\quad \hat{p}=\frac{p}{R\rho_{av}T_0},$$

where ρ_{av} is the average density of the gas between the cylinders. Therefore, $\hat{\rho}$ is normalized as

$$\frac{2}{(r_O/r_I)^2-1}\int_1^{r_O/r_I}\hat{r}\hat{\rho}\,d\hat{r}=1. \qquad (2)$$

Then, the Boltzmann equation in the dimensionless form reads

$$\zeta_r\frac{\partial\hat{f}}{\partial\hat{r}}+\frac{\zeta_\theta^2}{\hat{r}}\frac{\partial\hat{f}}{\partial\zeta_r}-\frac{\zeta_r\zeta_\theta}{\hat{r}}\frac{\partial\hat{f}}{\partial\zeta_\theta}=\frac{2}{\sqrt{\pi}\mathrm{Kn}}\hat{J}(\hat{f},\hat{f}), \qquad (3)$$

*Electronic address: aoki@aero.mbox.media.kyoto-u.ac.jp

$$\mathrm{Kn}=l_0/r_I, \tag{4}$$

where $\hat{J}(\hat{f},\hat{f})$ is the dimensionless collision term, the explicit form of which is given in Appendix A, Kn is the Knudsen number, and l_0 is the mean free path of the gas molecules in the equilibrium state at rest at density ρ_{av} and temperature T_0. For hard-sphere molecules, l_0 is given by $l_0=(\sqrt{2}\pi d^2\rho_{av}/m)^{-1}$, m and d being the mass and diameter of a molecule.

The boundary conditions on the cylinders are written as follows: on the inner cylinder (at $\hat{r}=1$), for $\zeta_r>0$,

$$\hat{f}(1,\boldsymbol{\zeta})=(1-\alpha_I)\hat{f}(1,-\zeta_r,\zeta_\theta,\zeta_z)+\alpha_I\frac{\sigma_I}{\pi^{3/2}}\exp[-\zeta_r^2-(\zeta_\theta-\hat{V}_I)^2-\zeta_z^2], \tag{5a}$$

$$\sigma_I=-2\sqrt{\pi}\int_{\zeta_r<0}\zeta_r\hat{f}(1,\boldsymbol{\zeta})d\boldsymbol{\zeta}, \tag{5b}$$

and on the outer cylinder (at $\hat{r}=r_O/r_I$), for $\zeta_r<0$,

$$\hat{f}(r_O/r_I,\boldsymbol{\zeta})=(1-\alpha_O)\hat{f}(r_O/r_I,-\zeta_r,\zeta_\theta,\zeta_z)+\alpha_O\frac{\sigma_O}{\pi^{3/2}}\exp(-\zeta_r^2-\zeta_\theta^2-\zeta_z^2), \tag{6a}$$

$$\sigma_O=2\sqrt{\pi}\int_{\zeta_r>0}\zeta_r\hat{f}(r_O/r_I,\boldsymbol{\zeta})d\boldsymbol{\zeta}, \tag{6b}$$

where α_I and α_O are the accommodation coefficient of the inner cylinder and that of the outer cylinder, respectively, and $d\boldsymbol{\zeta}=d\zeta_r d\zeta_\theta d\zeta_z$.

The macroscopic quantities $\hat{\rho}$, $\hat{v}_\theta$, $\hat{T}$, and $\hat{p}$ are given by

$$\hat{\rho}=\int\hat{f}d\boldsymbol{\zeta},\quad \hat{v}_\theta=\frac{1}{\hat{\rho}}\int\zeta_\theta\hat{f}d\boldsymbol{\zeta},$$
$$\hat{T}=\frac{2}{3\hat{\rho}}\int[\zeta_r^2+(\zeta_\theta-\hat{v}_\theta)^2+\zeta_z^2]\hat{f}d\boldsymbol{\zeta},\quad \hat{p}=\hat{\rho}\hat{T}. \tag{7}$$

Here and in what follows, the domain of integration with respect to $\boldsymbol{\zeta}$ is its whole space unless the contrary is stated.

It should be noted that the local Maxwellian distribution corresponding to the solid-body rotation [9] with $\hat{v}_\theta=\hat{V}_I\hat{r}$, i.e.,

$$\hat{f}=\frac{\hat{\rho}_0}{\pi^{3/2}}\exp(\hat{V}_I^2\hat{r}^2)\exp[-\zeta_r^2-(\zeta_\theta-\hat{V}_I\hat{r})^2-\zeta_z^2], \tag{8}$$

where $\hat{\rho}_0$ is a constant determined by Eq. (2), is the exact solution of the present problem when $\alpha_I\neq 0$ and $\alpha_O=0$. In view of this fact, one can naturally think that the inverted velocity profile (i.e., $\hat{v}_\theta$ increasing with $\hat{r}$) takes place when α_O becomes small. Our interest is to see the transition from the normal profile (i.e., $\hat{v}_\theta$ decreasing with $\hat{r}$) to the inverted one at small accommodation coefficients.

III. ASYMPTOTIC ANALYSIS FOR SMALL KNUDSEN NUMBERS

In this section we consider the case where the accommodation coefficients α_I and α_O, as well as the Knudsen number Kn, are small and carry out a systematic asymptotic analysis of the boundary-value problem (3) and (5a)–(6b), following Refs. [10–13] as a guideline. To begin with, we assume that α_I and α_O are of the order of Kn; that is, we put

$$\alpha_I=\beta_I\epsilon,\quad \alpha_O=\beta_O\epsilon,\quad \epsilon=(\sqrt{\pi}/2)\mathrm{Kn}\ll 1, \tag{9}$$

where β_I and β_O are given constants, and ϵ is a small parameter (of the order of Kn) that is mainly used in this section. Our aim is to derive a set of fluid-dynamic equations and its appropriate boundary conditions in the leading order, i.e., the order of Kn^0 (or ϵ^0). Since the method of the asymptotic analysis is described in detail in the recent monograph by Sone [13], we give only the brief outline of the analysis and show the main result.

A. Fluid-dynamic equation

First, putting aside the boundary conditions (5a)–(6b), we look for a moderately varying solution $\hat{f}_H$, satisfying $\partial\hat{f}_H/\partial\hat{r}=O(\hat{f}_H)$, in the form of a power series of ϵ:

$$\hat{f}_H=\hat{f}_{H0}+\hat{f}_{H1}\epsilon+\hat{f}_{H2}\epsilon^2+\cdots. \tag{10}$$

This $\hat{f}_H$ is called the Hilbert solution or expansion. Let $\hat{\rho}_H$, $\hat{v}_{\theta H},\ldots,$ be the macroscopic quantities $\hat{\rho}$, $\hat{v}_\theta,\ldots,$ corresponding to the Hilbert solution. Then, they are also expanded as

$$h_H=h_{H0}+h_{H1}\epsilon+h_{H2}\epsilon^2+\cdots, \tag{11}$$

where h represents $\hat{\rho}$, $\hat{v}_\theta$, $\hat{T}$, or $\hat{p}$. The explicit expressions of h_{Hm} in terms of $\hat{f}_{Hm}$ are obtained by substituting $\hat{f}=\hat{f}_H$ and $h=h_H$ in Eq. (7) and by equating the coefficients of the same power of ϵ.

If we substitute Eq. (10) into Eq. (3) and arrange the power of ϵ, we obtain a sequence of integral equations for the coefficients $\hat{f}_{Hm}$, which can be solved from the lowest order. For the leading-order term $\hat{f}_{H0}$, we have $\hat{J}(\hat{f}_{H0},\hat{f}_{H0})=0$, which means that $\hat{f}_{H0}$ is a local Maxwellian distribution. As for the higher-order term $\hat{f}_{Hm}$, we obtain a linear integral equation, containing the collision term $\hat{J}$ linearized around $\hat{f}_{H0}$, with inhomogeneous terms consisting of the earlier terms $\hat{f}_{Hn}$ $(n<m)$ of the Hilbert expansion. Since the corresponding homogeneous equation has the summational invariants (multiplied by $\hat{f}_{H0}$) as nontrivial solutions, the inhomogeneous terms should satisfy solvability conditions, which are reduced to the form

$$\int \begin{bmatrix} 1 \\ \boldsymbol{\zeta} \\ \zeta^2 \end{bmatrix} \left(\zeta_r \frac{\partial \hat{f}_{Hm}}{\partial \hat{r}} + \frac{\zeta_\theta^2}{\hat{r}} \frac{\partial \hat{f}_{Hm}}{\partial \zeta_r} - \frac{\zeta_r \zeta_\theta}{\hat{r}} \frac{\partial \hat{f}_{Hm}}{\partial \zeta_\theta} \right) d\boldsymbol{\zeta} = 0, \tag{12}$$

where

$$\zeta = |\boldsymbol{\zeta}| = (\zeta_r^2 + \zeta_\theta^2 + \zeta_z^2)^{1/2}. \tag{13}$$

The application of this condition to $\hat{f}_{H0}$, $\hat{f}_{H1}$, . . . , in the successive solution process of the sequence of the integral equations from the lowest order leads to the fluid-dynamic equations for h_{Hm} in Eq. (11).

To summarize, $\hat{f}_{H0}$ is obtained as

$$\hat{f}_{H0} = \frac{\hat{\rho}_{H0}}{(\pi \hat{T}_{H0})^{3/2}} \exp\left(- \frac{\zeta_r^2 + (\zeta_\theta - \hat{v}_{\theta H0})^2 + \zeta_z^2}{\hat{T}_{H0}} \right), \tag{14}$$

and $\hat{f}_{H1}$ as the form given in Appendix B [Eq. (B1)]. The fluid-dynamic equations in the leading order, i.e., those for $\hat{\rho}_{H0}$, $\hat{v}_{\theta H0}$, $\hat{T}_{H0}$, and $\hat{p}_{H0}$, are obtained in the following form:

$$\frac{d\hat{p}_{H0}}{d\hat{r}} - \frac{2\hat{\rho}_{H0}\hat{v}_{\theta H0}^2}{\hat{r}} = 0, \tag{15a}$$

$$\frac{d}{d\hat{r}} \left[\gamma_1 \hat{r}^2 \hat{T}_{H0}^{1/2} \left(\frac{d\hat{v}_{\theta H0}}{d\hat{r}} - \frac{\hat{v}_{\theta H0}}{\hat{r}} \right) \right] = 0, \tag{15b}$$

$$\frac{5}{4} \frac{d}{d\hat{r}} \left(\gamma_2 \hat{r} \hat{T}_{H0}^{1/2} \frac{d\hat{T}_{H0}}{d\hat{r}} \right) + \gamma_1 \hat{r} \hat{T}_{H0}^{1/2} \left(\frac{d\hat{v}_{\theta H0}}{d\hat{r}} - \frac{\hat{v}_{\theta H0}}{\hat{r}} \right)^2 = 0, \tag{15c}$$

$$\hat{p}_{H0} = \hat{\rho}_{H0} \hat{T}_{H0}, \tag{15d}$$

where γ_1 and γ_2 are functions of $\hat{T}_{H0}$ and their functional form depends on the molecular model (see Appendix B); for hard-sphere molecules, they are constants given by $\gamma_1 = 1.270\,042$, $\gamma_2 = 1.922\,284$; for the BGK model, $\gamma_1 = \gamma_2 = \hat{T}_{H0}^{1/2}$. $\gamma_1 \hat{T}_{H0}^{1/2}$ and $\gamma_2 \hat{T}_{H0}^{1/2}$ are, respectively, the dimensionless viscosity and thermal conductivity. Equations (15a)–(15d) are equivalent to the compressible Navier-Stokes equations. The appropriate boundary conditions for this set of equations are derived in the following subsection.

B. Knudsen layers and fluid-dynamic boundary conditions

Now we take into account the boundary conditions that were put aside in the preceding subsection. The boundary conditions (5a)–(6b) with Eq. (9) can be recast as

$$\hat{f}(\hat{r}_w, \boldsymbol{\zeta}) = (1 - \epsilon\beta_w) \mathcal{S}[\hat{f}(\hat{r}_w, \boldsymbol{\zeta})] + \epsilon\beta_w \mathcal{D}[\hat{f}(\hat{r}_w, \boldsymbol{\zeta})] \quad \text{for} \quad \delta_w \zeta_r > 0, \tag{16}$$

where, $\hat{r}_w$ represents 1 and r_O/r_I, and β_w and δ_w are as follows:

$$\beta_w = \beta_I, \quad \delta_w = 1, \quad \text{for} \quad \hat{r}_w = 1, \tag{17a}$$

$$\beta_w = \beta_O, \quad \delta_w = -1, \quad \text{for} \quad \hat{r}_w = r_O/r_I. \tag{17b}$$

In addition, the operators $\mathcal{S}$ and $\mathcal{D}$ are defined by

$$\mathcal{S}[\hat{f}(\hat{r}_w, \boldsymbol{\zeta})] = \hat{f}(\hat{r}_w, -\zeta_r, \zeta_\theta, \zeta_z), \tag{18a}$$

$$\mathcal{D}[\hat{f}(\hat{r}_w, \boldsymbol{\zeta})] = -\frac{2}{\pi} \int_{\delta_w \zeta_r < 0} \delta_w \zeta_r \hat{f}(\hat{r}_w, \boldsymbol{\zeta}) d\boldsymbol{\zeta} \times \exp(-\zeta_r^2 - (\zeta_\theta - \hat{V}_w)^2 - \zeta_z^2), \tag{18b}$$

where

$$\hat{V}_w = \begin{cases} \hat{V}_I & \text{for} \quad \hat{r}_w = 1 \\ 0 & \text{for} \quad \hat{r}_w = r_O/r_I. \end{cases} \tag{19}$$

Since $\hat{f}_{H0}$ is a local Maxwellian given by Eq. (14), it satisfies the specular-reflection condition on the cylinders, i.e.,

$$\hat{f}_{H0} = \mathcal{S}[\hat{f}_{H0}]. \tag{20}$$

In other words, it satisfies Eq. (16) in the leading order. However, as in the usual situation [13], the terms of $O(\epsilon)$ of condition (16) cannot be satisfied by the next-order term $\hat{f}_{H1}$ of the Hilbert expansion. To obtain the solution satisfying the boundary condition, therefore, we need to introduce the so-called Knudsen layers.

Let us seek the solution in the form

$$\hat{f} = \hat{f}_H + \hat{f}_K, \tag{21}$$

with

$$\hat{f}_K = \hat{f}_{K1}\epsilon + \hat{f}_{K2}\epsilon^2 + \cdots. \tag{22}$$

Here, $\hat{f}_K$ is the correction to the Hilbert solution $\hat{f}_H$ appreciable only in the thin layers of thickness of the order of ϵ (or of the mean free path in the dimensional r variable) adjacent to the cylinders (Knudsen layers). Expansion (22) is started from ϵ order because $\hat{f}_{H0}$ could satisfy the boundary condition in the leading order.

To handle the two Knudsen layers on the inner and outer cylinders in a unified way, we introduce the following variables:

$$y = \hat{r} - 1, \quad \eta = y/\epsilon, \quad \zeta_n = \zeta_r, \tag{23}$$

near the inner cylinder ($\hat{r} = 1$); and

$$y = r_O/r_I - \hat{r}, \quad \eta = y/\epsilon, \quad \zeta_n = -\zeta_r, \tag{24}$$

near the outer cylinder ($\hat{r} = r_O/r_I$). Here, y is the normal coordinate measured from each cylinder toward the gas, and

η is the stretched normal coordinate. We suppose that the length scale of variation of $\hat{f}_K$ is ϵ, i.e.,

$$\hat{f}_K = \hat{f}_K(\eta, \zeta_n, \zeta_\theta, \zeta_z) \tag{25}$$

or $\partial \hat{f}_K / \partial \eta = O(\hat{f}_K)$, and that $\hat{f}_K$ vanishes rapidly as $\eta \to \infty$.

If we substitute Eq. (21) [with Eqs. (10) and (22)] into Eqs. (3) and (16) and take into account the explicit forms of $\hat{f}_{H0}$ and $\hat{f}_{H1}$ as well as the properties of $\hat{f}_K$, we obtain the equation and boundary conditions for $\hat{f}_{K1}$, which are summarized as follows.

$$\zeta_n \frac{\partial \hat{f}_{K1}}{\partial \eta} = 2\hat{J}((\hat{f}_{H0})_w, \hat{f}_{K1}), \tag{26a}$$

$$\hat{f}_{K1} = \mathcal{S}[\hat{f}_{K1}] + \mathcal{S}[(\hat{f}_{H1})_w] - (\hat{f}_{H1})_w - \beta_w \mathcal{S}[(\hat{f}_{H0})_w] + \beta_w \mathcal{D}[(\hat{f}_{H0})_w] \quad \text{for} \quad \zeta_n > 0, \quad \text{at} \quad \eta = 0, \tag{26b}$$

$$\hat{f}_{K1} \to 0, \quad \text{as} \quad \eta \to \infty, \tag{26c}$$

where $(\,)_w$ indicates the value of the Hilbert solution at $y = 0$, i.e., at $\hat{r} = \hat{r}_w$, and $\hat{J}(\hat{f}, \hat{g})$ is defined by Eq. (A1) in Appendix A. Equations (26a)–(26c) are essentially the half-space boundary-value problem of the linearized Boltzmann equation.

Let us denote any of 1, $\boldsymbol{\zeta}$, and ζ^2 by Ψ. If we multiply Eq. (26a) by Ψ and integrate it over the whole space of $\boldsymbol{\zeta}$, we have $(\partial/\partial\eta)\int \Psi \zeta_n \hat{f}_{K1} d\boldsymbol{\zeta} = 0$ because of the property of the collision integral $\hat{J}$. Condition (26c) then gives

$$\int \Psi \zeta_n \hat{f}_{K1} d\boldsymbol{\zeta} = 0 \quad \text{for} \quad \eta \geqslant 0. \tag{27}$$

We now consider Eq. (27) on the boundary $\eta = 0$, using Eq. (26b) with the explicit forms of $\hat{f}_{H0}$ and $\hat{f}_{H1}$ for $\zeta_n > 0$ in the integral. Then we find that Eq. (27) with $\Psi = \zeta_\theta$ and ζ^2 gives two compatibility conditions for the boundary values of the leading-order terms h_{H0} [Eq. (11)] and of their derivatives. [Equation (27) with $\Psi = 1$ and ζ_z is automatically satisfied, whereas that with $\Psi = \zeta_n$ does not give any additional condition, consisting only of the boundary values of h_{H0} and dh_{H0}/dy.] The two compatibility conditions, arranged in an appropriate form for each cylinder, are given as follows: on the inner cylinder (at $\hat{r} = 1$),

$$\sqrt{\pi}\gamma_1 \left(\frac{d\hat{v}_{\theta H0}}{d\hat{r}} - \hat{v}_{\theta H0} \right) + \beta_I \hat{\rho}_{H0}(\hat{V}_I - \hat{v}_{\theta H0}) = 0, \tag{28a}$$

$$\frac{5}{4}\sqrt{\pi}\gamma_2 \frac{d\hat{T}_{H0}}{d\hat{r}} - \beta_I \hat{\rho}_{H0}(\hat{T}_{H0} - 1) + \frac{1}{2}\beta_I \hat{\rho}_{H0}(\hat{V}_I - \hat{v}_{\theta H0})^2 = 0, \tag{28b}$$

and on the outer cylinder (at $\hat{r} = r_O/r_I$),

$$\sqrt{\pi}\gamma_1 \left(-\frac{d\hat{v}_{\theta H0}}{d\hat{r}} + \frac{\hat{v}_{\theta H0}}{r_O/r_I} \right) - \beta_O \hat{\rho}_{H0} \hat{v}_{\theta H0} = 0, \tag{29a}$$

$$-\frac{5}{4}\sqrt{\pi}\gamma_2 \frac{d\hat{T}_{H0}}{d\hat{r}} - \beta_O \hat{\rho}_{H0}(\hat{T}_{H0} - 1) + \frac{1}{2}\beta_O \hat{\rho}_{H0}(\hat{v}_{\theta H0})^2 = 0. \tag{29b}$$

In deriving Eqs. (28b) and (29b) from Eq. (27) with $\Psi = \zeta^2$, Eqs. (28a) and (29a) have been used. Equations (28a)–(29b) give the boundary conditions for the fluid-dynamic equations (15a)–(15d).

In this way, the boundary conditions for the leading-order fluid-dynamic equations (15a)–(15d) are obtained from the first-order Knudsen-layer problem (26a)–(26c). At the same time, it should be noted that the former boundary conditions can be derived without solving the latter problem. This procedure to determine fluid-dynamic boundary conditions in the case of a small accommodation coefficient or specularly reflecting boundary was first devised in Ref. [14], where the thermal creep along a specularly reflecting wall was clarified. Then, it was applied in Refs. [15] and [16], where the fluid-dynamic system for small Knudsen numbers was derived for the general geometry with a specularly [15] or almost specularly [16] reflecting boundary when the system was close to a uniform equilibrium state at rest. The existence and uniqueness of a solution of a half-space problem that contains the problem (26a)–(26c) as a special case have been proved by Golse *et al.* [17].

As is easily seen in the course of analysis, if the accommodation coefficients are of the order of unity [i.e., $\alpha_I = O(1)$ and $\alpha_O = O(1)$], the boundary conditions for Eqs. (15a)–(15d) become the so-called nonslip conditions:

$$\hat{v}_{\theta H0} = \hat{V}_I, \quad \hat{T}_{H0} = 1, \quad \text{at} \quad \hat{r} = 1, \qquad \hat{v}_{\theta H0} = 0, \quad \hat{T}_{H0} = 1, \quad \text{at} \quad \hat{r} = r_O/r_I. \tag{30}$$

These can be obtained formally by letting $\beta_I \to \infty$ in Eq. (28) and $\beta_O \to \infty$ in Eq. (29).

C. Flow properties at small Knudsen numbers

We have derived the fluid-dynamic equations (15a)–(15d) and their boundary conditions (28a)–(29b) for the leading order in Kn (or ϵ) under assumption (10). Some numerical results of this system for hard-sphere molecules are shown in Fig. 1. That is, the velocity profile $\hat{v}_{\theta H0}$ is shown in the case where $\beta_I = \beta_O = \beta$, $r_O/r_I = 2$, and $\hat{V}_I = V_I/(2RT_0)^{1/2} = 0.1$ [(a)], 0.3 [(b)], and 0.5 [(c)]. The dashed line in Fig. 1(c) indicates the solution given by Eq. (34) below [see the sentences following Eq. (34)]. In the figures, the inverted velocity profile is observed for $\beta \leqslant 0.5$.

Since the above system cannot be solved analytically, we consider the case where the rotation speed is small (but much larger than the Knudsen number). More specifically, we assume that $\hat{V}_I \ll 1$ and thus $\hat{v}_{\theta H0} \ll 1$ ($\hat{V}_I$ and $\hat{v}_{\theta H0}$ are supposed to be positive). Correspondingly, we put $\hat{\rho}_{H0} = 1 + \omega$,

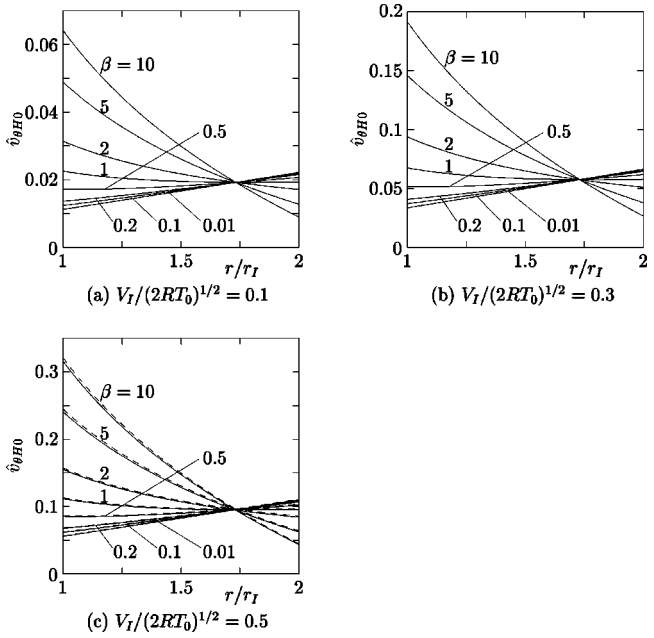

FIG. 1. Velocity profile given by the fluid-dynamic system (15a)–(15d) and (28a)–(29b) for hard-sphere molecules. The $\hat{v}_{\theta H0}$ versus $r/r_I(=\hat{r})$ is shown for various values of $\beta_I=\beta_O=\beta$ and three values of $V_I/(2RT_0)^{1/2}(=\hat{V}_I)$ in the case of $r_O/r_I=2$. (a) $V_I/(2RT_0)^{1/2}=0.1$, (b) $V_I/(2RT_0)^{1/2}=0.3$, (c) $V_I/(2RT_0)^{1/2}=0.5$. The dashed line in (c) indicates the solution given by Eq. (34).

$\hat{T}_{H0}=1+\tau$, and $\hat{p}_{H0}=1+P$ with $|\omega|\ll 1$, $|\tau|\ll 1$, and $|P|\ll 1$. Incidentally, we write $\hat{v}_{\theta H0}=u\ll 1$. Note that $\mathrm{Kn}\ll\{\text{any of } \hat{V}_I,\ u,\ |\omega|,\ |\tau|,\text{ and } |P|\}\ll 1$. Then, if we neglect the higher-order terms, Eqs. (15a)–(15d) reduce to

$$\frac{dP}{d\hat{r}}=0, \tag{31a}$$

$$\frac{d}{d\hat{r}}\left[\hat{r}^2\left(\frac{du}{d\hat{r}}-\frac{u}{\hat{r}}\right)\right]=0, \tag{31b}$$

$$\frac{d}{d\hat{r}}\left(\hat{r}\frac{d\tau}{d\hat{r}}\right)=0, \tag{31c}$$

$$P=\omega+\tau, \tag{31d}$$

and boundary conditions (28a)–(29b) to the following: on the inner cylinder (at $\hat{r}=1$),

$$\sqrt{\pi}\gamma_1^*\left(\frac{du}{d\hat{r}}-u\right)+\beta_I(\hat{V}_I-u)=0, \tag{32a}$$

$$\frac{5}{4}\sqrt{\pi}\gamma_2^*\frac{d\tau}{d\hat{r}}-\beta_I\tau=0, \tag{32b}$$

and on the outer cylinder (at $\hat{r}=r_O/r_I$),

$$\sqrt{\pi}\gamma_1^*\left(-\frac{du}{d\hat{r}}+\frac{u}{r_O/r_I}\right)-\beta_O u=0, \tag{33a}$$

$$-\frac{5}{4}\sqrt{\pi}\gamma_2^*\frac{d\tau}{d\hat{r}}-\beta_O\tau=0, \tag{33b}$$

where γ_1^* and γ_2^* are γ_1 and γ_2 at $\hat{T}_{H0}=1$, respectively. This system can be solved readily and gives

$$u=A\hat{r}^{-1}+B\hat{r},\quad \omega=\tau=P=0, \tag{34}$$

where

$$A=\frac{1}{D}\frac{r_O}{r_I}\beta_I\beta_O\hat{V}_I, \tag{35a}$$

$$B=\frac{1}{D}\left[2\sqrt{\pi}\gamma_1^*\left(\frac{r_I}{r_O}\right)^2-\frac{r_I}{r_O}\beta_O\right]\beta_I\hat{V}_I, \tag{35b}$$

$$D=\left(\frac{r_O}{r_I}-\frac{r_I}{r_O}\right)\beta_I\beta_O+2\sqrt{\pi}\gamma_1^*\left[\frac{r_O}{r_I}\beta_O+\left(\frac{r_I}{r_O}\right)^2\beta_I\right]. \tag{35c}$$

Equation (34) corresponds to the solution of the incompressible Navier-Stokes equations. It should be noted that the pressure gradient due to the centrifugal force appears in the higher order, so that there is no pressure gradient in the leading order [Eq. (31a)]. Solution (34) is also plotted in Fig. 1(c) (dashed line). Even for $\hat{V}_I=0.5$, the difference between the solution of the compressible system and Eq. (34) is very small. If the latter is plotted in Fig. 1(a), the difference is invisible.

If we assume the specular-reflection condition on both cylinders from the beginning [i.e., if $\alpha_I=\alpha_O=0$ in Eqs. (5a) and (6a)], the solution is indeterminate because the solid-body rotation with an arbitrary angular speed [Eq. (8) with $\hat{V}_I$ replaced by an arbitrary constant] is a solution. On the contrary, if we take the limit $\beta_I\to 0$ and $\beta_O\to 0$, keeping the ratio $\chi=\beta_O/\beta_I$ fixed, in Eq. (34), then we have $u\to\hat{V}_I\hat{r}/[1+(r_O/r_I)^3\chi]$, that is, the limiting flow is the solid-body rotation with an angular speed determined uniquely by ratio χ.

D. Continuum limit

In this subsection, we comment briefly on the continuum limit. The continuum limit is the limit where the Knudsen number Kn (or ϵ) vanishes. In this limit, because of Eq. (9), the boundary conditions on both cylinders approach the specular reflection. On the other hand, we have $\hat{\rho}\to\hat{\rho}_{H0}$, $\hat{v}_\theta\to\hat{v}_{\theta H0}$, $\hat{T}\to\hat{T}_{H0}$, and $\hat{p}\to\hat{p}_{H0}$ in this limit because the Knudsen-layer correction appears in the order of ϵ. This means that the continuum limit of the Couette flow for the specular-reflection condition is uniquely determined if the limit is taken appropriately, i.e., in such a way that α_I and α_O vanish in proportion to ϵ [Eq. (9)], and the limiting solution depends on the proportionality constants (β_I and β_O).

In contrast, if α_I and α_O are set to be zero from the beginning, the solution is indeterminate for any Kn including the continuum limit. Finally, if the continuum limit Kn$\to$0 is taken for any fixed α_I and α_O, then the limiting solution is given by the solution of Eqs. (15a)–(15d) with the nonslip condition (30) even when α_I and α_O are small.

IV. CASE OF FREE-MOLECULAR FLOW

Next, we consider the other extreme case where the Knudsen number is infinitely large, i.e., the free-molecular flow. In this case, one can obtain the exact solution to the original system, Eq. (3) (with the right-hand side equal to zero) and boundary conditions (5a)–(6b), in the following form:

$$\hat{f}(\hat{r},\boldsymbol{\zeta})=\frac{C}{\pi^{3/2}}\exp(-\zeta_\rho^2-\zeta_z^2)\quad(\varphi<|\theta_\zeta|<\pi-\varphi), \tag{36a}$$

$$\hat{f}(\hat{r},\boldsymbol{\zeta})=\frac{\alpha_I(1-\alpha_O)}{\alpha_I+\alpha_O-\alpha_I\alpha_O}\frac{C}{\pi^{3/2}}\exp(-\zeta_\rho^2+2\hat{r}\hat{V}_I\zeta_\rho\sin\theta_\zeta-\zeta_z^2-\hat{V}_I^2)+\frac{\alpha_O}{\alpha_I+\alpha_O-\alpha_I\alpha_O}\frac{C}{\pi^{3/2}}\exp(-\zeta_\rho^2-\zeta_z^2)\quad(\pi-\varphi<|\theta_\zeta|<\pi), \tag{36b}$$

$$\hat{f}(\hat{r},\boldsymbol{\zeta})=\frac{\alpha_I}{\alpha_I+\alpha_O-\alpha_I\alpha_O}\frac{C}{\pi^{3/2}}\exp(-\zeta_\rho^2+2\hat{r}\hat{V}_I\zeta_\rho\sin\theta_\zeta-\zeta_z^2-\hat{V}_I^2)+\frac{\alpha_O(1-\alpha_I)}{\alpha_I+\alpha_O-\alpha_I\alpha_O}\frac{C}{\pi^{3/2}}\exp(-\zeta_\rho^2-\zeta_z^2)\quad(0<|\theta_\zeta|<\varphi), \tag{36c}$$

where

$$\zeta_\rho=(\zeta_r^2+\zeta_\theta^2)^{1/2},\quad \theta_\zeta=\arctan(\zeta_\theta/\zeta_r),\quad \varphi=\arcsin(1/\hat{r}), \tag{37}$$

and C is a constant. Then, the macroscopic quantities are obtained from Eqs. (7) and (36) as follows:

$$\hat{\rho}(\hat{r})=\frac{C}{\pi}\left(\pi-2\varphi+\frac{2\alpha_O-\alpha_I\alpha_O}{\alpha_I+\alpha_O-\alpha_I\alpha_O}\varphi\right)+\frac{2\alpha_I-\alpha_I\alpha_O}{\alpha_I+\alpha_O-\alpha_I\alpha_O}\frac{C}{\pi}\exp(-\hat{V}_I^2)\times\left[\varphi+\sqrt{\pi}\int_0^\varphi\Theta\exp(\Theta^2)\operatorname{erf}\Theta\,d\theta_\zeta\right], \tag{38}$$

$$\hat{v}_\theta(\hat{r})=\frac{2\alpha_I-\alpha_I\alpha_O}{\alpha_I+\alpha_O-\alpha_I\alpha_O}\frac{C}{\hat{\rho}\pi}\exp(-\hat{V}_I^2)\left[\frac{\hat{V}_I\hat{r}}{4}(2\varphi-\sin 2\varphi)+\sqrt{\pi}\int_0^\varphi\left(\Theta^2+\frac{1}{2}\right)\exp(\Theta^2)\operatorname{erf}\Theta\sin\theta_\zeta\,d\theta_\zeta\right], \tag{39}$$

$$\hat{T}(\hat{r})=\frac{1}{3}-\frac{2}{3}\hat{v}_\theta^2+\frac{2C}{3\hat{\rho}\pi}\left(\pi-2\varphi+\frac{2\alpha_O-\alpha_I\alpha_O}{\alpha_I+\alpha_O-\alpha_I\alpha_O}\varphi\right)+\frac{2\alpha_I-\alpha_I\alpha_O}{\alpha_I+\alpha_O-\alpha_I\alpha_O}\frac{2C}{3\hat{\rho}\pi}\exp(-\hat{V}_I^2)\times\left[\frac{\hat{V}_I^2\hat{r}^2}{4}(2\varphi-\sin 2\varphi)+\varphi+\sqrt{\pi}\int_0^\varphi\left(\Theta^3+\frac{3}{2}\Theta\right)\exp(\Theta^2)\operatorname{erf}\Theta\,d\theta_\zeta\right], \tag{40}$$

where $\Theta=\hat{V}_I\hat{r}\sin\theta_\zeta$, and $\operatorname{erf}z=(2/\sqrt{\pi})\int_0^z\exp(-t^2)dt$ is the error function. Constant C in Eqs. (36) and (38)–(40) is determined by Eq. (2). In the derivation of the above solution, we have assumed that $\alpha_O\neq 0$. It should be noted that when $\alpha_I=\alpha_O$, all the macroscopic quantities are independent of the accommodation coefficient, though the velocity distribution function still depends on it. Results (38)–(40) will be shown in some figures in Sec. V.

V. NUMERICAL ANALYSIS FOR WHOLE RANGE OF KNUDSEN NUMBER

Finally, we consider the case of arbitrary Knudsen numbers. Here, we use two different numerical approaches: one is the stochastic method known as the direct simulation Monte Carlo (DSMC) method [18,19] and the other is a deterministic finite-difference method based on the BGK model. We hereafter restrict ourselves to the case where the accommodation coefficients are common to both cylinders and put $\alpha_I=\alpha_O=\alpha$.

A. Monte Carlo simulation

We start with the DSMC computation. Since the method is widely used and described in many places (see, e.g., Refs. [20–22] in addition to Refs. [18,19]), we give only the result of analysis, omitting the description of the solution process. In this subsection, we assume that the gas molecules are hard spheres. In the actual computation, we use 200 uniform cells in $r_I<r<r_O$ and 200 simulation particles per cell on the average.

Figure 2 shows some results for $r_O/r_I=2$ and $V_I/(2RT_0)^{1/2}(=\hat{V}_I)=0.5$. More specifically, the velocity profile $v_\theta/(2RT_0)^{1/2}(=\hat{v}_\theta)$ is plotted for various values of α $(=\alpha_I=\alpha_O)$ in the case of Kn=0.02, 0.05, 0.1, 1, 10, and 100. Note that the Reynolds number Re$=(4/\sqrt{\pi}\gamma_1)(\hat{V}_I/\mathrm{Kn})$ (cf. Ref. [13]) in the present computation, which is less than 45, is below the critical Reynolds number for the Taylor-Couette instability [23] so the flow is axially

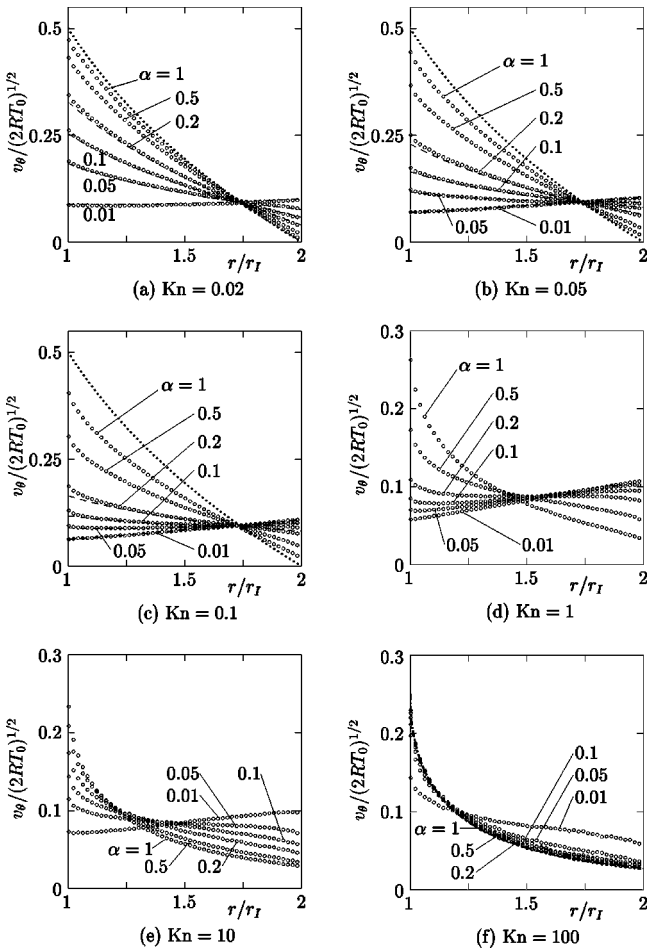

FIG. 2. The numerical result by the DSMC method for hard-sphere molecules: velocity profile. The $v_\theta/(2RT_0)^{1/2}$ is shown for various values of $\alpha_I=\alpha_O=\alpha$ and Kn in the case of $r_O/r_I=2$ and $V_I/(2RT_0)^{1/2}=0.5$. (a) Kn=0.02, (b) Kn=0.05, (c) Kn=0.1, (d) Kn=1, (e) Kn=10, (f) Kn=100. In (a)–(c), the dashed line indicates the numerical solution of Eqs. (15a)–(15d) with boundary conditions (28a)–(29b), and the dotted line that of the same equations with the nonslip conditions (30). In (f), the thick dot-dashed line indicates the free-molecular flow solution (39), which is independent of α.

and circumferentially uniform (see also Ref. [24]). In Figs. 2(a)–2(c) [Kn=0.02, 0.05, and 0.1], the numerical solution of the fluid-dynamic system for small α and Kn, i.e., Eqs. (15a)–(15d) and (28a)–(29b), is shown by the dashed line for $\alpha=0.01$, 0.05, 0.1, and 0.2, and the numerical solution of Eqs. (15a)–(15d) and (30) (nonslip condition) is shown by the dotted line. In Fig. 2(f) (Kn=100), the free-molecular-flow result, Eq. (39), is shown by the thick dot-dashed line. For Kn=1, the inverted velocity profile is observed for $\alpha \leqslant 0.1$, but it is limited to smaller α when Kn is either small or large. For small Kn and α, the fluid-dynamic solution shows good agreement with the DSMC result, so that the dashed lines in Figs. 2(a)–2(c) are not seen clearly. For Kn=100, the profile is weakly dependent on α, which is consistent with the free-molecular-flow result, and thus the inverted velocity profile is not observed even for $\alpha=0.01$. The range of α for the inverted profile will be discussed in the following subsection.

B. Finite-difference analysis of the BGK model

In order to obtain more detailed information on the parameter range for the inverted velocity profile, we carry out a deterministic numerical analysis using the BGK model rather than the original Boltzmann equation. We employ the finite-difference method developed by Sone and Sugimoto in their study of strong evaporation from spherical and cylindrical condensed phases [25–27].

A difficulty inherent in the finite-difference analysis is caused by the fact that the molecular velocity distribution function around a convex body generally contains discontinuities [28]. The method mentioned above is capable of describing the behavior of the discontinuity around a spherical or cylindrical body. In the present problem, the situation is slightly more complicated because the discontinuity caused by the inner cylinder, in general, reaches the outer cylinder and is reflected there by the specular-reflection part of the boundary condition (6a). Therefore, we need to adjust the above-mentioned scheme to the present problem. But, since the method is essentially the same as that described in detail in Refs. [25–27], we give only the result of the analysis.

Figure 3 shows the velocity profile for the BGK model, corresponding to Fig. 2. The meaning of the dashed and dotted lines in Figs. 3(a)–3(c) is the same as in Fig. 2, but the relation $\gamma_1=\gamma_2=\hat{T}_{H0}^{1/2}$, which corresponds to the BGK model, is used in Eqs. (15a)–(15d) and (28a)–(29b). Figures 4 and 5 show, respectively, the density and temperature profiles for the BGK model for typical Kn in the same case as in Fig. 3. Figure 3 is very similar to Fig. 2, though there is a small quantitative discrepancy.

As is seen from Figs. 2 and 3, the velocity profile is monotonically decreasing when α is close to unity. If α is decreased for a fixed Kn, the monotonicity ceases at a relatively small α, say, α_c, i.e., the profile exhibits a local minimum when $\alpha<\alpha_c$. Then, with the further decrease of α, the profile becomes monotonically increasing. We show the critical value α_c versus Kn for the BGK model in Fig. 6, where $r_O/r_I=2$ and $V_I/(2RT_0)^{1/2}=0.1$ and 0.5. The α_c is almost the same for both values of $V_I/(2RT_0)^{1/2}$ and becomes largest at Kn=0.7∼0.8. From Eq. (34), we have the following α_c for small Kn and small $V_I/(2RT_0)^{1/2}$[Kn $\ll V_I/(2RT_0)^{1/2} \ll 1$]:

$$\alpha_c=(\pi/2)(r_I/r_O)\gamma_1^*\ \mathrm{Kn}. \tag{41}$$

This result for the BGK model ($\gamma_1^*=1$) is also shown by the solid line in Fig. 6. The range of parameters, α and Kn, for which the profile exhibits a local minimum is within the reach of laboratory experiments [29].

Here, we comment on the comparison between the result for hard-sphere molecules and that for the BGK model. As is well known, the way of comparison between the results for different molecular models is not unique. One of the standard ways is the following. The viscosity coefficient μ_0 corresponding to the reference density ρ_{av} and temperature T_0 is

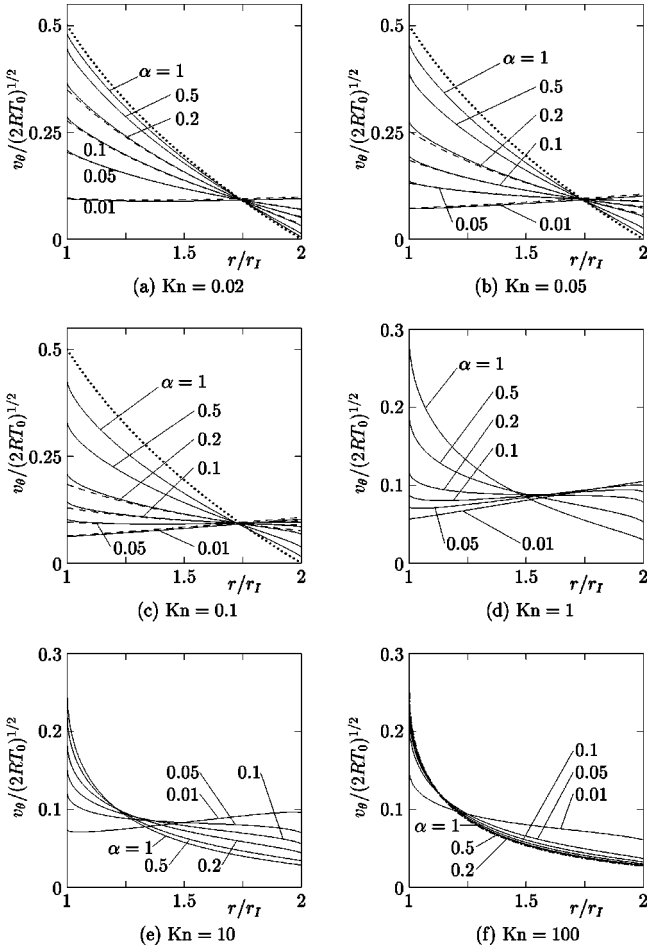

FIG. 3. The numerical result by the finite-difference method for the BGK model: velocity profile. The $v_\theta/(2RT_0)^{1/2}$ is shown for various values of $\alpha_I=\alpha_O=\alpha$ and Kn in the case of $r_O/r_I=2$ and $V_I/(2RT_0)^{1/2}=0.5$. (a) Kn=0.02, (b) Kn=0.05, (c) Kn=0.1, (d) Kn=1, (e) Kn=10, (f) Kn=100. In (a)–(c), the dashed line indicates the numerical solution of Eqs. (15a)–(15d) with boundary conditions (28a)–(29b), and the dotted line that of the same equations with the nonslip conditions (30). In (f), the thick dot-dashed line indicates the free-molecular flow solution (39), which is independent of α.

given by $\mu_0=(\sqrt{\pi}/4)\gamma_1^*\rho_{av}(2RT_0)^{1/2}l_0$ (cf. Sec. 3.9 of Ref. [13]). If we suppose that μ_0 is a fundamental quantity and is common to all the molecular models, then we obtain the relations among the mean free paths or the Knudsen numbers for the different molecular models. In the case of hard-sphere molecules and the BGK model, we have the following relationship:

$$l_{0(\mathrm{BGK})}=1.270\,042\,l_{0(\mathrm{HS})},$$
$$\mathrm{Kn}_{(\mathrm{BGK})}=1.270\,042\,\mathrm{Kn}_{(\mathrm{HS})}, \tag{42}$$

where the suffixes (BGK) and (HS) indicate the quantities for the BGK model and those for hard-sphere molecules, respectively. In Fig. 7, we compare the velocity profile for the BGK model with that for hard-sphere molecules in the case where $r_O/r_I=2$, $V_I/(2RT_0)^{1/2}=0.5$, and $\mathrm{Kn}_{(\mathrm{HS})}=0.1$,

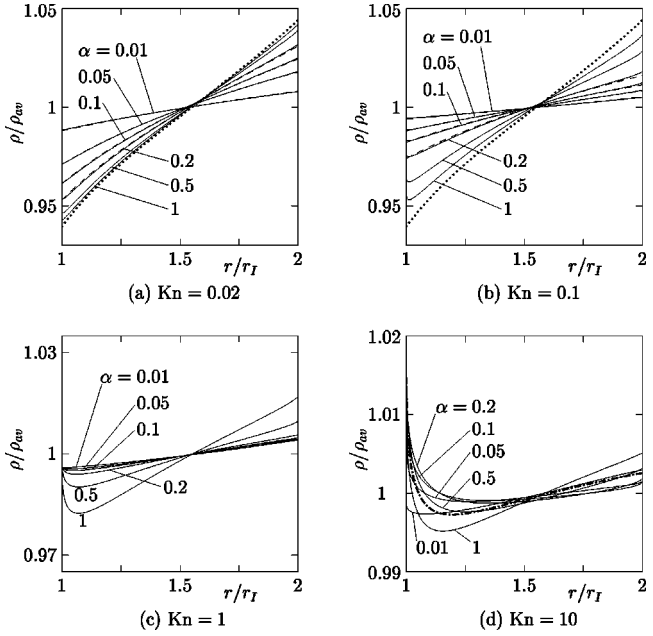

FIG. 4. The numerical result by the finite-difference method for the BGK model: density profile. The ρ/ρ_{av} is shown for various values of $\alpha_I=\alpha_O=\alpha$ and typical values of Kn in the case of $r_O/r_I=2$ and $V_I/(2RT_0)^{1/2}=0.5$. (a) Kn=0.02, (b) Kn=0.1, (c) Kn=1, (d) Kn=10. In (a) and (b), the dashed line indicates the numerical solution of Eqs. (15a)–(15d) with boundary conditions (28a)–(29b), and the dotted line that of the same equations with the nonslip conditions (30). In (d), the thick dot-dashed line indicates the free-molecular flow solution (39), which is independent of α.

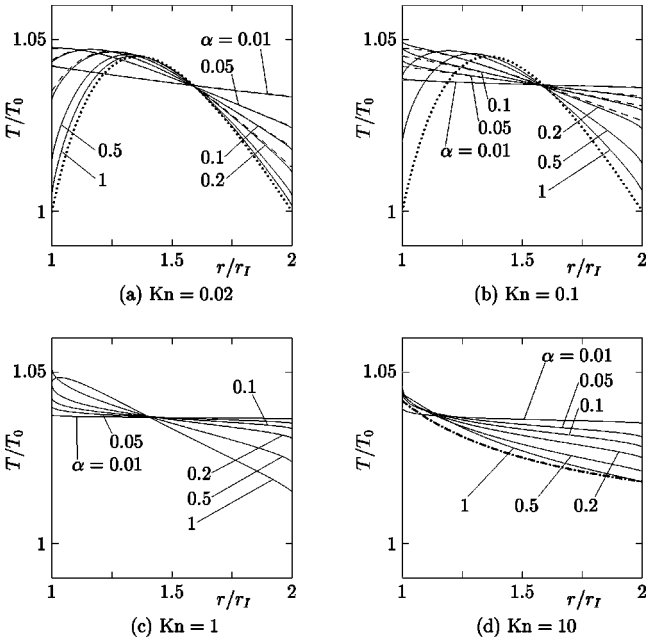

FIG. 5. The numerical result by the finite-difference method for the BGK model: temperature profile. The T/T_0 is shown for various values of $\alpha_I=\alpha_O=\alpha$ and typical values of Kn in the case of $r_O/r_I=2$ and $V_I/(2RT_0)^{1/2}=0.5$. (a) Kn=0.02, (b) Kn=0.1, (c) Kn=1, (d) Kn=10. See the caption of Fig. 4.

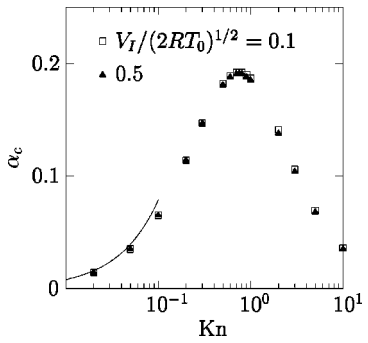

FIG. 6. The critical accommodation coefficient α_c versus Kn for the BGK model in the case of $r_O/r_I=2$ and $V_I/(2RT_0)^{1/2}=0.1$ and 0.5. The solid curve indicates Eq. (41).

using the conversion formula (42). More specifically, the result at $\mathrm{Kn}=0.127\,004\,2$ for the BGK model is compared with that at $\mathrm{Kn}=0.1$ for hard-sphere molecules. The figure shows very good agreement.

The data for the computational system in the finite-difference analysis are as follows. Region $1\leqslant\hat{r}\leqslant r_O/r_I$ is divided into 240 nonuniform intervals (the minimum size is 4.284×10^{-5} at the cylinders, and the maximum size is 6.545×10^{-3} around $\hat{r}=1.5$); region $0\leqslant\zeta_\rho<\infty$ [see Eq. (37)] is replaced by $0\leqslant\zeta_\rho\leqslant6.912$ and then divided into 48 nonuniform intervals (the minimum size is 6.25×10^{-5} at $\zeta_\rho=0$, and the maximum size 0.4231 at $\zeta_\rho=6.912$); region $-\pi\leqslant\theta_\zeta\leqslant\pi$ [see Eq. (37)] is divided into 272 uniform intervals (note that ζ_z can be eliminated by suitable integration in the case of the BGK model [25,27]).

VI. CONCLUDING REMARKS

In the present study, we investigated the cylindrical Couette flow of a rarefied gas between two coaxial circular cylinders in the case where the inner cylinder is rotating whereas the outer one is at rest. The diffuse-specular reflection condition of Maxwell's type was assumed on the cylinders. Special attention was focused on the inverted velocity profile (the velocity profile increasing with the distance from the inner cylinder) for small accommodation coefficients observed previously by the Monte Carlo simulation [6]. After the formulation of the problem in Sec. II, we first considered the near continuum case in Sec. III, where we derived the fluid-dynamic system for small accommodation coefficients by means of a systematic asymptotic analysis of the Boltzmann equation and showed that the system describes the inverted velocity profile. Next, we considered the other extreme case, the free-molecular-flow limit, in Sec. IV and derived the analytical solution. In this case, the macroscopic quantities do not depend on the accommodation coefficients if they are common to both cylinders. Finally in Sec. V, we carried out numerical analysis of the original Boltzmann system for a wide range of the Knudsen number by using two different approaches: one is the Monte Carlo simulation (DSMC method) for hard-sphere molecules and the other is a deterministic finite-difference analysis of the BGK model. On the basis of these numerical results, the range of the accommodation coefficients that gives the inverted velocity profiles (more precisely, the profile that is not monotonically decreasing) was clarified for certain cases of the driving parameters [$\alpha_I=\alpha_O=\alpha$, $r_O/r_I=2$, and $V_I/(2RT_0)^{1/2}=0.1$ and 0.5].

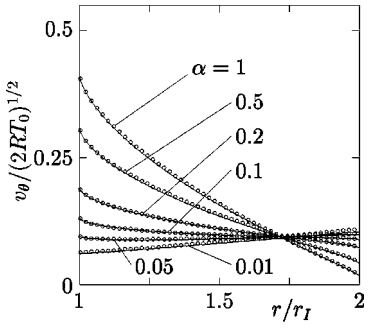

FIG. 7. The comparison between the result for the BGK model and that for hard-sphere molecules using conversion (42). The $v_\theta/(2RT_0)^{1/2}$ versus r/r_I is shown for $r_O/r_I=2$, $V_I/(2RT_0)^{1/2}=0.5$, and $\mathrm{Kn}_{(\mathrm{HS})}=0.1$. The solid line indicates the result for the BGK model, and the symbol ○ that for hard-sphere molecules.

To conclude the paper, we discuss the inverted velocity profile from a qualitative, physical point of view. The rotating inner cylinder imparts the circumferential component of the momentum to the diffusely reflected molecules. When α_I is small, the rate of the transfer of the circumferential momentum is small, but it is supplied continuously. When Kn is small, the circumferential momentum is transferred to the entire gas by molecular collisions. If the outer cylinder is specularly reflecting ($\alpha_O=0$), the circumferential momentum is not transferred to the outer cylinder. In other words, there is no braking effect by the outer cylinder. Then, the gas is accelerated until solid-body rotation, in which the transfer of the circumferential momentum vanishes, is established. This situation, in which the velocity profile is inverted since $v_\theta\propto r$, corresponds to Eq. (8). When α_O is small but nonzero, some of the circumferential momentum is transferred to the outer cylinder by the diffusely reflected molecules, and its reaction brakes the rotation of the gas near the outer cylinder. But, if the braking effect is small, the velocity profile remains inverted, as in solid-body rotation. The numerical result shows that this is the case when $\alpha_I=\alpha_O$ and they are sufficiently small. When Kn is sufficiently large ($\mathrm{Kn}\gg1$), a competing effect arises: because collisions in the gas are rare, most of the circumferential momentum imparted to the diffusely reflected molecules on the inner cylinder is transferred not to the gas but to the outer cylinder directly. Therefore, in contrast to the case of small Kn, the gas away from the inner cylinder is not accelerated. In this case, the number of the molecules with higher speed in the circumferential direction is larger near the inner cylinder, so that the inversion of the velocity profile does not appear.

ACKNOWLEDGMENT

This work was supported by a Grant-in-Aid for Scientific Research (Grant No. 14350047) from the Japan Society for the Promotion of Science.

APPENDIX A: COLLISION INTEGRAL

The collision integral $\hat{J}(\hat{f},\hat{f})$ is defined by the following bilinear integral operator $\hat{J}(\hat{f},\hat{g})$:

$$\hat{J}(\hat{f},\hat{g})=\frac{1}{2}\int(\hat{f}'\hat{g}'_*+\hat{f}'_*\hat{g}'-\hat{f}\hat{g}_*-\hat{f}_*\hat{g})\hat{B}d\Omega d\boldsymbol{\zeta}_*, \tag{A1a}$$

$$\hat{B}=\hat{B}(|\boldsymbol{V}\cdot\mathbf{e}|/|\boldsymbol{V}|,|\boldsymbol{V}|), \quad \boldsymbol{V}=\boldsymbol{\zeta}_*-\boldsymbol{\zeta}, \tag{A1b}$$

$$\boldsymbol{\zeta}'=\boldsymbol{\zeta}+(\boldsymbol{V}\cdot\mathbf{e})\mathbf{e}, \quad \boldsymbol{\zeta}'_*=\boldsymbol{\zeta}_*-(\boldsymbol{V}\cdot\mathbf{e})\mathbf{e}, \tag{A1c}$$

where $\hat{f}'$, $\hat{f}'_*$, $\hat{f}$, and $\hat{f}_*$ stand for $\hat{f}(\boldsymbol{\zeta})$ with $\boldsymbol{\zeta}=\boldsymbol{\zeta}'$, $\boldsymbol{\zeta}'_*$, $\boldsymbol{\zeta}$, and $\boldsymbol{\zeta}_*$, respectively, and the same for $\hat{g}$; $\boldsymbol{\zeta}_*$ is the variable of integration corresponding to $\boldsymbol{\zeta}$, and $\mathbf{e}$ is a unit vector; $\hat{B}$ is a non-negative function of $|\boldsymbol{V}\cdot\mathbf{e}|/|\boldsymbol{V}|$ and $|\boldsymbol{V}|$ depending on the molecular model (for hard-sphere molecules, $\hat{B}=|\boldsymbol{V}\cdot\mathbf{e}|/4\sqrt{2\pi}$); $d\Omega$ is the solid-angle element around $\mathbf{e}$, and $d\boldsymbol{\zeta}_*=d\zeta_{*r}d\zeta_{*\theta}d\zeta_{*z}$; the domain of integration in Eq. (A1a) is all directions of $\mathbf{e}$ and the whole space of $\boldsymbol{\zeta}_*$. (See Sec. 2.9 in Ref. [13].)

In the BGK model, the collision term $\hat{J}(\hat{f},\hat{f})$ is replaced by the following $\hat{J}_{\mathrm{BGK}}(\hat{f})$:

$$\hat{J}_{\mathrm{BGK}}(\hat{f})=\hat{\rho}(\hat{f}_e-\hat{f}), \tag{A2a}$$

$$\hat{f}_e=\frac{\hat{\rho}}{(\pi\hat{T})^{3/2}}\exp\left(-\frac{\zeta_r^2+(\zeta_\theta-\hat{v}_\theta)^2+\zeta_z^2}{\hat{T}}\right), \tag{A2b}$$

where $\hat{\rho}$, $\hat{v}_\theta$, and $\hat{T}$ are given in Eq. (7) [$\hat{v}_r=\hat{v}_z=0$ is used in Eq. (A2b)].

APPENDIX B: HILBERT SOLUTION $\hat{f}_{H1}$

The first-order Hilbert solution $\hat{f}_{H1}$ is obtained in the following form:

$$\begin{aligned}\hat{f}_{H1}=\hat{f}_{H0}\Bigg[&\frac{\hat{\rho}_{H1}}{\hat{\rho}_{H0}}+\frac{2\hat{v}_{\theta H1}\tilde{\zeta}_\theta}{\hat{T}_{H0}^{1/2}}+\frac{\hat{T}_{H1}}{\hat{T}_{H0}}\left(\tilde{\zeta}^2-\frac{3}{2}\right)\\&-\frac{1}{\hat{p}_{H0}}\frac{d\hat{T}_{H0}}{d\hat{r}}\tilde{\zeta}_r\mathcal{A}(\tilde{\zeta},\hat{T}_{H0})-\frac{\hat{T}_{H0}^{1/2}}{\hat{p}_{H0}}\\&\times\left(\frac{d\hat{v}_{\theta H0}}{d\hat{r}}-\frac{\hat{v}_{\theta H0}}{\hat{r}}\right)\tilde{\zeta}_r\tilde{\zeta}_\theta\mathcal{B}(\tilde{\zeta},\hat{T}_{H0})\Bigg],\end{aligned} \tag{B1}$$

where

$$\tilde{\zeta}_r=\frac{\zeta_r}{\hat{T}_{H0}^{1/2}}, \quad \tilde{\zeta}_\theta=\frac{\zeta_\theta-\hat{v}_{\theta H0}}{\hat{T}_{H0}^{1/2}}, \quad \tilde{\zeta}_z=\frac{\zeta_z}{\hat{T}_{H0}^{1/2}}, \tag{B2a}$$

$$\tilde{\zeta}=(\tilde{\zeta}_r^2+\tilde{\zeta}_\theta^2+\tilde{\zeta}_z^2)^{1/2}. \tag{B2b}$$

The functions $\mathcal{A}$ and $\mathcal{B}$ are the solutions of the following integral equations:

$$\left.\begin{aligned}&\mathcal{L}_T(\zeta_r\mathcal{A}(\zeta,\hat{T}_{H0}))=-\zeta_r\left(\zeta^2-\frac{5}{2}\right),\\&\text{subsidiary condition:}\\&\int_0^\infty\zeta^4\mathcal{A}(\zeta,\hat{T}_{H0})\exp(-\zeta^2)d\zeta=0,\end{aligned}\right\} \tag{B3}$$

$$\mathcal{L}_T(\zeta_r\zeta_\theta\mathcal{B}(\zeta,\hat{T}_{H0}))=-2\zeta_r\zeta_\theta, \tag{B4}$$

where $\zeta=(\zeta_r^2+\zeta_\theta^2+\zeta_z^2)^{1/2}$ [Eq. (13)], and $\mathcal{L}_T(\phi(\boldsymbol{\zeta}))$ is the linearized collision operator defined by $\mathcal{L}_a(\phi(\boldsymbol{\zeta}))$ in Ref. [13] [Eq. (A.23) in Sec. A.2 of Appendix A there] with $a=\hat{T}_{H0}$, i.e.,

$$\mathcal{L}_T(\phi(\boldsymbol{\zeta}))=\int E(\zeta_*)(\phi'+\phi'_*-\phi-\phi_*)\hat{B}_T d\Omega d\boldsymbol{\zeta}_*, \tag{B5a}$$

$$\hat{B}_T=\hat{T}_{H0}^{-1/2}\hat{B}(|\boldsymbol{V}\cdot\mathbf{e}|/|\boldsymbol{V}|,\hat{T}_{H0}^{1/2}|\boldsymbol{V}|), \tag{B5b}$$

$$E(\zeta)=\pi^{-3/2}\exp(-\zeta^2), \tag{B5c}$$

$$\zeta_*=(\zeta_{*r}^2+\zeta_{*\theta}^2+\zeta_{*z}^2)^{1/2}, \tag{B5d}$$

where ϕ', ϕ'_*, ϕ, and ϕ_* stand for $\phi(\boldsymbol{\zeta})$ with $\boldsymbol{\zeta}=\boldsymbol{\zeta}'$, $\boldsymbol{\zeta}'_*$, $\boldsymbol{\zeta}$, and $\boldsymbol{\zeta}_*$ [cf. Eq. (A1c)], respectively. The coefficients γ_1 and γ_2 occurring in the fluid-dynamic equations [Eqs. (15b) and (15c)] are expressed in terms of the functions $\mathcal{A}$ and $\mathcal{B}$ as follows:

$$\gamma_1(\hat{T}_{H0})=\frac{8}{15\sqrt{\pi}}\int_0^\infty\zeta^6\mathcal{B}(\zeta,\hat{T}_{H0})\exp(-\zeta^2)d\zeta, \tag{B6a}$$

$$\gamma_2(\hat{T}_{H0})=\frac{16}{15\sqrt{\pi}}\int_0^\infty\zeta^6\mathcal{A}(\zeta,\hat{T}_{H0})\exp(-\zeta^2)d\zeta. \tag{B6b}$$

Since $\mathcal{L}_T$ generally depends on $\hat{T}_{H0}$ and the molecular model, functions $\mathcal{A}$ and $\mathcal{B}$ and thus γ_1 and γ_2 also depend on them. In the case of hard-sphere molecules, $\mathcal{A}$, $\mathcal{B}$, γ_1, and γ_2 are independent of $\hat{T}_{H0}$ and are given by [13]

$$\mathcal{A}(\zeta,\hat{T}_{H0})=A(\zeta), \quad \mathcal{B}(\zeta,\hat{T}_{H0})=B(\zeta), \tag{B7a}$$

$$\gamma_1=1.270\,042, \quad \gamma_2=1.922\,284. \tag{B7b}$$

Functions $A(\zeta)$ and $B(\zeta)$ are given in Table 3.1 in Ref. [13]. For the BGK model, these quantities are given as [13]

$$\mathcal{A}(\zeta,\hat{T}_{H0})=\hat{T}_{H0}^{1/2}\left(\zeta^2-\frac{5}{2}\right), \quad \mathcal{B}(\zeta,\hat{T}_{H0})=2\hat{T}_{H0}^{1/2}, \tag{B8a}$$

$$\gamma_1=\gamma_2=\hat{T}_{H0}^{1/2}. \tag{B8b}$$

[1] C. Cercignani and F. Sernagiotto, Phys. Fluids **10**, 1200 (1967).
[2] F. Sharipov and G. Kremer, Eur. J. Mech. B/Fluids **15**, 493 (1996).
[3] Y. Sone, H. Sugimoto, and K. Aoki, Phys. Fluids **11**, 476 (1999).
[4] Y. Sone and T. Doi, Phys. Fluids **12**, 2639 (2000).
[5] Y. Sone, M. Handa, and H. Sugimoto, Transp. Theory Stat. Phys. **31**, 299 (2002).
[6] K.W. Tibbs, F. Baras, and A.L. Garcia, Phys. Rev. E **56**, 2282 (1997).
[7] P.L. Bhatnagar, E.P. Gross, and M. Krook, Phys. Rev. **94**, 511 (1954).
[8] P. Welander, Ark. Fys. **7**, 507 (1954).
[9] H. Grad, Commun. Pure Appl. Math. **2**, 331 (1949).
[10] Y. Sone, in *Rarefied Gas Dynamics*, edited by L. Trilling and H.Y. Wachman (Academic, New York, 1969), p. 243.
[11] Y. Sone, in *Rarefied Gas Dynamics*, edited by D. Dini (Editrice Tecnico Scientifica, Pisa, 1971), Vol. II, p. 737.
[12] Y. Sone, in *Advances in Kinetic Theory and Continuum Mechanics*, edited by R. Gatignol and J.B. Soubbaramayer (Springer, Berlin, 1991), p. 19.
[13] Y. Sone, *Kinetic Theory and Fluid Dynamics* (Birkhäuser, Boston, 2002).
[14] Y. Sone, J. Phys. Soc. Jpn. **29**, 1655 (1970).
[15] Y. Sone and K. Aoki, Phys. Fluids **20**, 571 (1977).
[16] K. Aoki, T. Inamuro, and Y. Onishi, J. Phys. Soc. Jpn. **47**, 663 (1979).
[17] F. Golse, B. Perthame, and C. Sulem, Arch. Ration. Mech. Anal. **103**, 81 (1988).
[18] G.A. Bird, *Molecular Gas Dynamics* (Oxford University Press, Oxford, 1976).
[19] G.A. Bird, *Molecular Gas Dynamics and the Direct Simulation of Gas Flows* (Oxford University Press, Oxford, 1994).
[20] C. Cercignani, *Rarefied Gas Dynamics, From Basic Concepts to Actual Calculations* (Cambridge University Press, Cambridge, 2000).
[21] A.L. Garcia, *Numerical Methods for Physics*, 2nd ed. (Prentice Hall, Upper Saddle River, NJ, 2000).
[22] Y. Sone, Y. Waniguchi, and K. Aoki, Phys. Fluids **8**, 2227 (1996).
[23] E.L. Koschmieder, *Bénard Cells and Taylor Vortices* (Cambridge University Press, Cambridge, 1993).
[24] K. Aoki, Y. Sone, and M. Yoshimoto, in *Rarefied Gas Dynamics*, edited by R. Brun, R. Campargue, R. Gatignol, and J.-C. Lengrand (Cépaduès-Éditions, Toulouse, 1999), Vol. 2, p. 109.
[25] H. Sugimoto and Y. Sone, Phys. Fluids A **4**, 419 (1992).
[26] Y. Sone and H. Sugimoto, Phys. Fluids A **5**, 1491 (1993).
[27] Y. Sone and H. Sugimoto, Phys. Fluids **7**, 2072 (1995).
[28] Y. Sone and S. Takata, Transp. Theory Stat. Phys. **21**, 501 (1992).
[29] F. O. Goodman and H. Y. Wachman, *Dynamics of Gas-Surface Scattering* (Academic, New York, 1976).